Enhancing Superchiral Fields and Circular Dichroism Detection by Achiral Dielectric Metasurfaces

Xianzhe Zhang[1], Chuangtang Wang[1], Renchao Jin[1], Zhaogang Dong[2,3,4,#], Yuri Kivshar[5,#], and Yongmin Liu[6,#]

[1]Department of Electrical and Computer Engineering, Northeastern University, Boston, Massachusetts 02115, USA

[2]Science, Mathematics, and Technology (SMT), Singapore University of Technology and Design (SUTD), 8 Somapah Road, Singapore 487372

[3]Institute of Materials Research and Engineering, Agency for Science, Technology and Research (A*STAR), 2 Fusionopolis Way, Innovis #08-03, Singapore 138634, Republic of Singapore

[4]Quantum Innovation Centre (Q.InC), Agency for Science Technology and Research (A*STAR), 2 Fusionopolis Way, Innovis #08-03, Singapore 138634, Republic of Singapore

[5]Nonlinear Physics Center, Research School of Physics, Australian National University, Canberra, Australian Capital Territory 2601, Australia

[6]Department of Mechanical and Industrial Engineering, Northeastern University, Boston, Massachusetts 02115, USA

[#] Corresponding author. Email: zhaogang_dong@sutd.edu.sg, yuri.kivshar@anu.edu.au, and y.liu@northeatern.edu

Abstract

In this work, we demonstrate that dielectric metasurfaces consisting of achiral silicon nanocube dimers can generate pronounced superchiral fields through engineering the electric and magnetic resonant modes. The superchiral fields exhibit over 20-fold enhancement of optical chirality density in the visible region. While previous studies have noted the presence of superchiral fields in both dielectric and metallic nanostructures, detecting and assessing local superchiral fields remains a challenging task. We show that the third Stokes parameter, readily obtainable from far-field measurements, can serve as an indicator of the strong chiral hot spot within the gap of an achiral silicon nanocube dimer. We further characterize the circular dichroism signals of D- and L-phenylalanine molecules in the presence of silicon nanocube dimers, revealing an approximately 12-fold increase compared to the control experiment conducted without nanocube dimers. The experimental and simulation results show good agreement. The all-dielectric achiral metasurface

paves a new way toward chiral molecule detection with the advantages of low loss, low background noise, and high sensitivity.

Keywords: circular dichroism, third Stokes parameter, superchiral field.

Introduction

Chirality is a fundamental concept with profound implications across the fields of chemistry, biology, and physics. A pair of chiral molecules, termed enantiomers, are mirror images of each other. They have identical molecular formulas but can show distinct responses and effects. For instance, individual enantiomers of chiral drugs may exhibit very disparate bioactivities and biotoxicities, and chiral pesticides can show significant differences in environmental activity and persistence.[1–4] Therefore, it is crucial to efficiently and accurately differentiate between enantiomers. One widely used technique to detect and analyze chirality is circularly dichroism (CD) spectroscopy, which measures the differential absorption of chiral molecules subject to the illumination of left-hand circularly polarized (LCP) and right-hand circularly polarized (RCP) light.[5]. However, the optical activity of naturally existing chiral entities is generally very weak, and therefore the chiral effect is detectable only when molecular concentration is sufficiently high, normally at the micro-molar level.

Over the past years, researchers have proposed and demonstrated various methods to enhance CD signals of molecules. These methods include the use of standing-wave-induced superchiral light,[6] dielectric-based platform[7–10], plasmonic resonances,[11–23] magnetic resonances,[24–26] nano-cavity resonators,[27–29] and fluorescence tags,[30–33] Despite the enhanced CD signals with some designated structures, these methods either introduce strong background noise from the chiral structure itself or suffer from the non-uniform chiral field distribution that hinders the global CD enhancement, causing issues such as limited sensitivity and amplitude fluctuations.

In this work, we demonstrate that dielectric metasurfaces composed of achiral silicon nanocube dimers can yield strong chiral hot spots for CD measurements. Silicon nanostructures, with their large refractive index, can support electric dipole, magnetic dipole, and higher-order resonances when excited by linearly polarized light (LPL) at visible wavelengths.[9,10] When the incidence becomes circularly polarized light (CPL), the overlapped electric and magnetic resonant modes generate a strong, uniform chiral hot spot in the gap of the nanocube dimers with maximized

average chirality if the proper phase condition is fulfilled[34–36]. We use the third Stokes parameters obtained from the far-field measurement to verify the local superchiral field, helping us reveal the fundamental mechanism of chiral light-matter interactions. Furthermore, we demonstrate that the achiral dielectric metasurface can achieve 12-fold enhancement in CD signals of D- and L-phenylalanine molecules in the experiment, reasonably agreeing with the predicted 50-fold enhancement from full-wave simulations. Table S1 in Section S1 of the Supporting Information compares our work with the relevant literature. We can see that our work not only achieve noticeable detection in an aqueous environment, but also show a low detection limit. We believe that our work would pave the way for enantioselective sensing, sorting, synthesis, and photolysis based on rationally designed nanophotonic structures with low loss and low background noise.

Results and Discussions

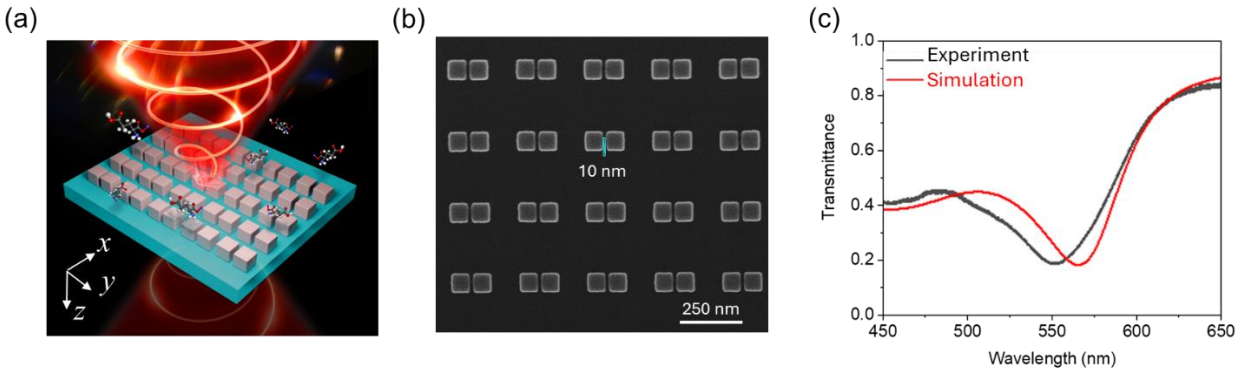

Figure 1. (a) Schematic of the silicon metasurface for chiral molecule sensing. (b) SEM image of a fabricated metasurface. (c) Measured and simulated transmittance spectra.

Figure 1(a) schematically shows the designed dielectric metasurfaces consisting of achiral silicon nanocube dimers. The length, width, and height of a nanocube are all 100 nm, and the gap between the nanocube dimer in a unit cell is 10 nm. The periodicity of the structure is 360 nm. Electron beam lithography (EBL) is used to fabricate the nanocube dimers. Briefly, we used the 100 keV EBL system to pattern the 25-nm hydrogen silsesquioxane (HSQ, Dow Corning XR-1541) on top of the 100-nm amorphous silicon film as grown by inductively coupled plasma (ICP) chemical vapor deposition (CVD) method, and followed by ICP etching with Cl_2 gas chemistry. **Figure 1(b)** presents the scanning electron microscope (SEM) image of a fabricated metasurface, from which we can see the high quality of the sample. **Figure 1(c)** plots the measured and simulated transmittance spectra, which show good agreement. The discrepancy is mainly attributed to the

imperfections in the sample fabrication process. The simulation details are provided in Section S2 in the Supporting Information.

To understand the underlying principle of chiral sensing, we start with the discussion of the chirality of an optical field, which is characterized by the optical chirality density C defined as[37,38]

$$C = \frac{\varepsilon_0}{2} E \cdot \nabla \times E + \frac{1}{2\mu_0} B \cdot \nabla \times B = -\frac{\omega \varepsilon_0}{2} Im(\boldsymbol{E}^* \cdot \boldsymbol{B}) \quad (1)$$

Here E ($\boldsymbol{E}$) is the real (complex) electric vector fields and B ($\boldsymbol{B}$) is the real (complex) magnetic vector fields, and ε_0 and μ_0 are the permittivity and permeability of the vacuum, respectively. For CPL in free space, the optical chirality density can be simplified to

$$C_0 = \pm \frac{\omega \varepsilon_0}{2c} |\boldsymbol{E}|^2 \quad (2)$$

where c is the speed of light in the vacuum and the sign depends on the handedness of CPL, that is, left-handed circularly polarized (LCP) or right-handed circularly polarized (RCP) light.

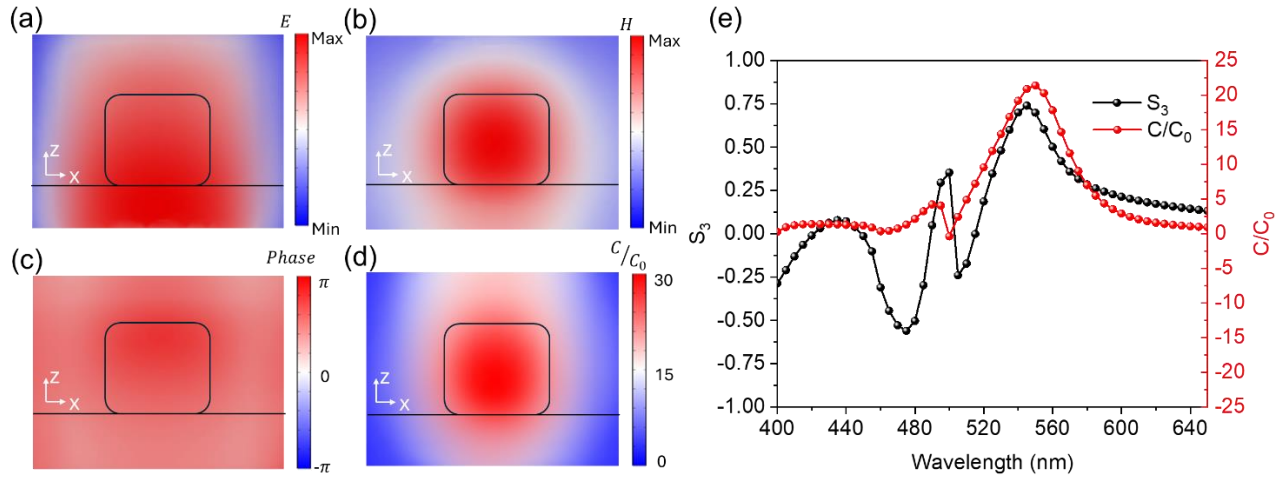

Figure 2. (a-d) Distribution of the electric field (a), the magnetic field (b), their relative phase (c), and the normalized optical chirality density (d), in the *xz*-plane cutting through the middle of the gap between two silicon nanocube dimers. The wavelength is 560 nm for all the plots. (e) Simulated third Stokes parameter (S_3, black curve) with linear polarized light, and the normalized optical chirality density (C/C_0, red curve) at the center of the gap of the dimer.

Equation (1) suggests that by overlapping the electric and magnetic fields and controlling their relative phase to be around $\pi/2$, we can produce a significantly enhanced superchiral field. Through multipole expansion analysis (see Section S3 in the Supporting Information), we can

identify that the silicon nanocube dimers can support electric dipole and magnetic dipole resonances centered around 480 nm and 550 nm, respectively. **Figure 2 (a)** and **2(b)** depict the distribution of the electric and magnetic fields, respectively, in the *yz*-plane cutting through the middle of the gap between two silicon nanocubes, when CPL illuminates the structure at the wavelength of 560 nm. **Figure 2(c)** presents the relative phase between the electric and magnetic fields. These results clearly show that we can satisfy the conditions to generate a superchiral field by engineering the electric and magnetic resonance of the silicon nancube dimers. Indeed, from **Figure 2(d)**, we can observe a hot spot of the optical chirality density in the dimer gap, exhibiting more than 20-fold enhancement. This makes it possible to provide an excellent platform to enhance CD signals once chiral molecules are adsorbed onto the dimers and experience the local chiral spot.

It is of great interest to understand the principle of this metasurface to be used for chiral sensing. Characterizing the superchiral field would help to reveal the underlying mechanism of the proposed platform for chiral sensing. Interestingly, we can resort to the third Stokes parameter (S_3), which can be readily measured in the far field, to probe the near-field chirality. The working principle can be understood by considering the optical chirality flux,[39] which is defined as

$$\mathcal{F} = \frac{1}{4\mu_0}[\boldsymbol{E} \times (\nabla \times \boldsymbol{B}^*) - \boldsymbol{B}^* \times (\nabla \times \boldsymbol{E})] \tag{3}$$

An electric field can be written as $\boldsymbol{E} = l\boldsymbol{E}_{LCP} + r\boldsymbol{E}_{RCP}$, where l and r denoted the weighting factors of LCP and RCP light. By applying Eq. (3) to LCP and RCP light, we can find that $\mathcal{F}$ is directly related to the power flux (S) in the following form

$$\mathcal{F} = \frac{\omega}{c}(|l|^2 S_{LCP} - |r|^2 S_{RCP}) \tag{4}$$

Therefore, $\mathcal{F}$ is proportional to the third Stokes parameter, an easily measurable far-field quantity that describes the degree of circular polarization. To further elucidate the physical implication of Eq. (4), in analogy to Poynting's theorem, Poulikakos *et al.* have formulated the conservation law of optical chirality in a lossy dispersive medium, which is given by [40],

$$-2\omega\int_V Im(\chi_e - \chi_m)d^3x + \int_V Re(\nabla \cdot \mathcal{F})d^3x = 0 \tag{4}$$

Here, χ_e and χ_m are the complex harmonic electric and magnetic optical chirality densities, respectively, which are given by[39]

$$\chi_e = \frac{\varepsilon_0}{8}[\boldsymbol{E}^* \cdot (\nabla \times \boldsymbol{E}) + \boldsymbol{E} \cdot (\nabla \times \boldsymbol{E}^*)] \quad (5)$$

$$\chi_m = \frac{1}{8\mu_0}[\boldsymbol{B}^* \cdot (\nabla \times \boldsymbol{B}) + \boldsymbol{B} \cdot (\nabla \times \boldsymbol{H}^*)] \quad (6)$$

From equation (4), one can find that the net chirality flux of linearly polarized light is zero because it is a superposition of LCP and RCP. In the measurement of the third Stokes parameters that will be discussed in the following, when linearly polarized light interacts with the silicon nanocube dimers and generates a chiral hot spot showing one specific handedness, one circular polarization state will be attenuated due to the preferential dissipation in the system. Based on the conservation law of optical chirality, a nonzero scattered chirality flux and hence a nonzero third Stokes parameter will be produced.[41] Furthermore, the sign of S_3 is related to the handedness of the local superchiral field and the incident light, while the amplitude of S_3 indicates how strong the chiral field is since it is directly proportional to the chirality flux. In **Figure 2 (e)**, we plot the simulated S_3 and the normalized optical chirality density, tha is, C/C_0. The spectra for both parameters show a very similar trend. Therefore, we conclude that the third Stokes parameter can serve as the far-field probe of the near-field chirality density.

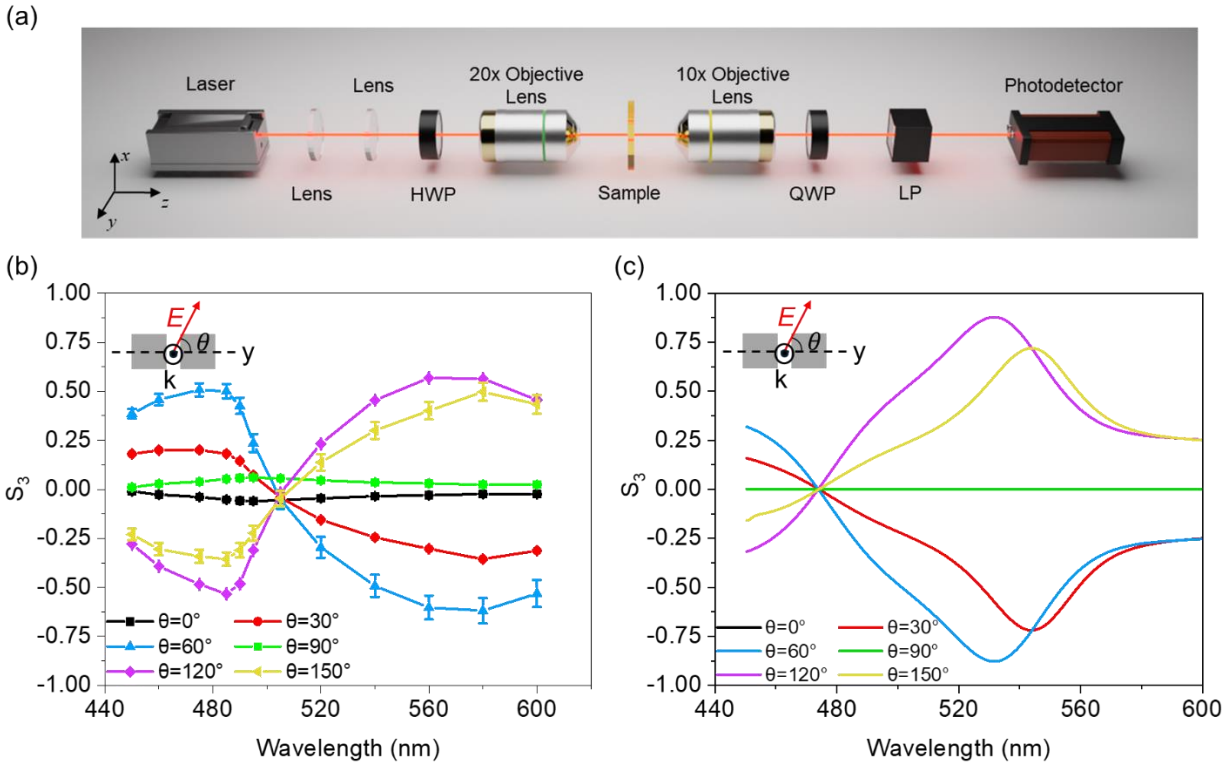

Figure 3. (a) Schematic of the optical setup to measure the third Stokes parameter. HWP: half-wave plate; QWP: quarter-wave plate; LP: linear polarizer. (b) Measured and (c) simulated third Stokes parameter when the polarization direction of the incident light is varied. The insets illustrate the polarization angle with respect to the long axis of the nanocube dimer.

Using a customized optical setup illustrated in **Figure 3(a)**, we measured the third Stokes parameter S_3. In the setup, a tunable laser (Coherent Chameleon Ultra II and Chameleon Compact OPO Vis-Idler) was used as the source. It was collimated by two lenses before it passed through a half-wave plate, which was used to vary the polarization direction of light impinging on the sample. Two objective lenses, with 20× and 10× magnification, respectively, were used to focus light on the silicon metasurface and collect the light transmitted through the metasurface. The diameter of the focused beam on the sample was approximately 20 μm. A quarter-wave plate and a linear polarizer were placed after the metasurface to obtain the S_3 spectra. From the measured S_3 spectra in **Figure 3(b)**, we can see that the curves are rather symmetric for two supplementary angles. S_3 remains essentially zero at all wavelengths when the polarization direction is parallel or perpendicular to the dimer axis. In this case, the superchiral field inside the gap cannot be excited, because the electric and magnetic dipoles are not simultaneously generated.[34] Specifically, an electric (or magnetic) hotspot emerges exclusively when the incident electric field is polarized parallel (or perpendicular) to the long dimer axis. Under this condition, the outgoing chiral flux is zero, and hence the third Stokes parameter remains zero for all wavelengths. In contrast, S_3 is nonzero (except around 500 nm wavelength) when the polarization direction of the incident light is off the dimer axis. In this case, the linearly polarized incidence, similar to CPL, can induce electric and magnetic dipoles simultaneously. The spatial overlap between the electric and magnetic dipoles and their $\pi/2$ relative phase difference ensures a chiral hotspot in the gap, producing a nonzero S_3 in the far field. The simulated S_3 spectra are depicted in **Figure 3(c)**, which generally agrees with the experimental results. The spectra show a blue shift, which is likely due to the imperfection in the fabrication. We have measured the S_3 parameter of other silicon nanocube dimers with different doses in the EBL process. The overall trend is very similar, while we can observe slight wavelength shifts in the spectra, because of the geometrical variations of the samples arising from different doses in the EBL process.

To further prove the feasibility of our chiral sensing platform, we conducted CD measurements on various molecules using the silicon metasurface as the experimental platform, after confirming the presence of the superchiral field. The measurement setup is illustrated in **Figure 4(a)**. A linear polarizer and a quarter waveplate wave placed before the sample to generate CPL. A convex lens with a focal length of 50 mm focused the laser beam onto the sample. After it passed through the sample, the laser was split into two beams by a beamsplitter, which were captured by a CCD camera and collected by a photodetector independently. The diameter of the focused beam on the sample was approximately 20 μm. In our experiment, we used a lock-in amplifier and a mechanical chopper to improve the signal-to-noise ratio and retrieve better CD spectra. For the CD measurements, we selected D-, L-, and DL-Phenylalanine. D-Phenylalanine exhibits right-handedness, L-Phenylalanine exhibits left-handedness, while DL-Phenylalanine is achiral. We used double-sided tape to create a 50 μm thick cavity between two slides. The solutions containing D-, L-, or DL-Phenylalanine could be held in the microcavity for ~7 hours before evaporation. This duration is sufficient to complete the measurements.

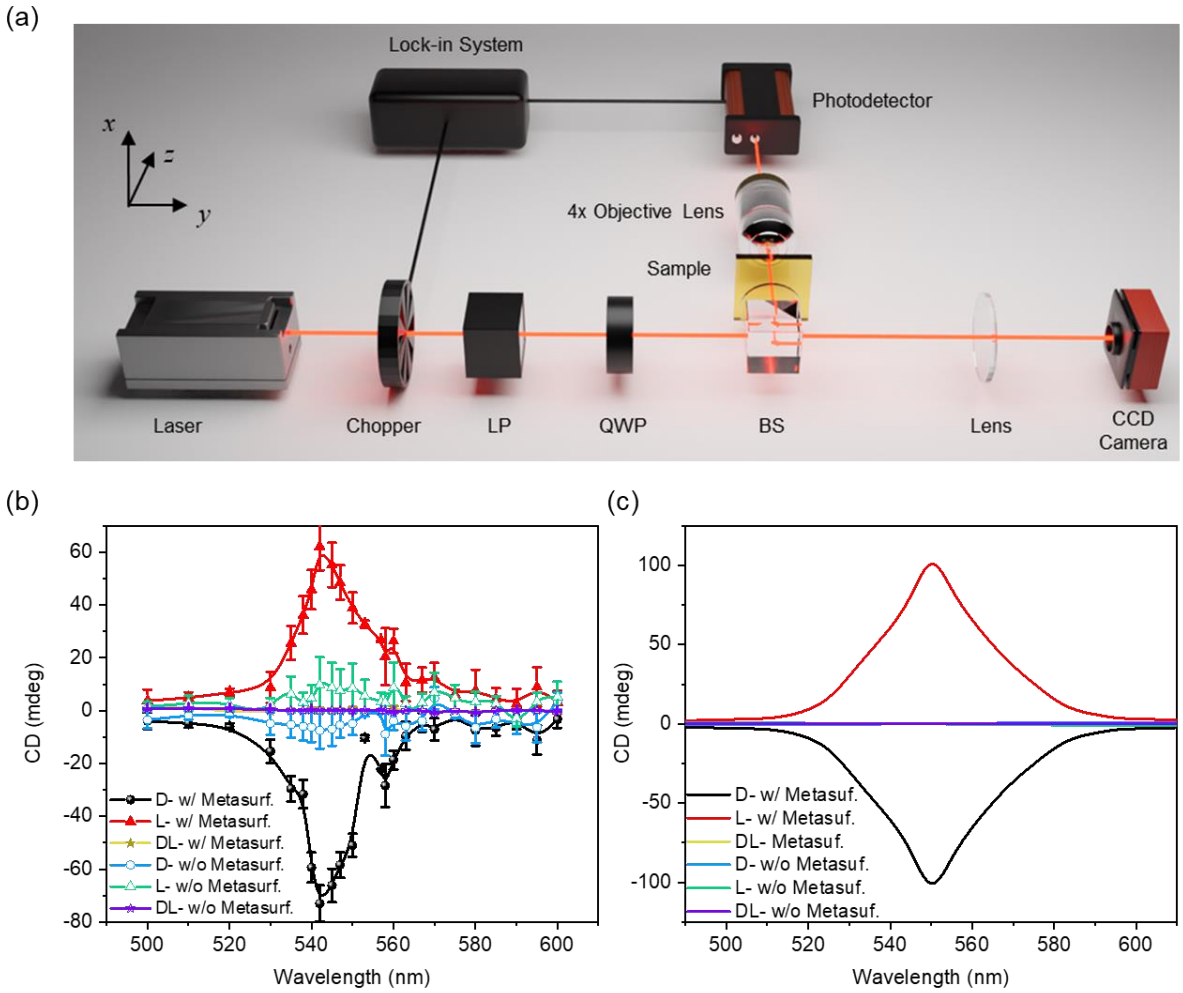

Figure 4. (a) Schematic of the optical setup to measure the CD spectra. LP: Linear Polarizer; QWP: Quarter-wave plate; BS: Beamsplitter. (b) Measured and (c) simulated CD spectra of molecules with or without metasurfaces. The error bar in the plot was calculated by standard derivation.

The expression to retrieve CD spectra is given by

$$CD = \arctan\left(\frac{T_{LCP}-T_{RCP}}{T_{LCP}+T_{RCP}}\right) \tag{7}$$

where T_{LCP} and T_{RCP} are the transmittance of LCP and RCP light through the sample, respectively. **Figure 4(b)** plots the measured CD spectra of different samples with molecule concentration of 30 $\mu g/ml$ in the wavelength range of 500-600 nm. The CD spectra of D- and L- Phenylalanine have reversed signs due to their opposite handedness. Within the visible regime, the intrinsic CD of D- and L-Phenylalanine is extremely small especially when it is dissolved into solutions.[42]

However, in the presence of silicon nanocube dimers, the chiral spot generated by the dimers can substantially enhance the CD signal by ~12 times at the resonance wavelength of 540 nm. Thanks to this enhancement, we can detect CD signals for molecules at a concentration as low as 5 $\mu g/ml$, yielding very good sensitivity (see Figure S3 in the Supporting Information). The simulated CD spectra of different molecules are shown in **Figure 4 (c)**. In the simulation, we represented the chiral molecules in the gap of the nanotube dimer as a thin chiral medium. The simulated CD enhancement is up to 50 times. Overall, there is good agreement between the simulated and measured CD spectra. As for the decrease in the amplitude, the slight wavelength shift, and the narrowing of the CD peaks in the experimental data, they are caused by the imperfection of the fabrication, the molecule distribution, simplification of the simulation, and bubbles in the cavity. In addition to molecules in solution, we performed the CD measurements using PMMA thin films mixed with D-phenylalanine. The experimental results are presented in Figure S4 in the Supporting Information, showing similar CD enhancement. The CD spectra of pure molecules in the UV regime are plotted in Figure S5 for reference.

Conclusions

In summary, we numerically and experimentally demonstrate the efficacy of achiral silicon metasurfaces in enhancing CD detection. Different from plasmonic nanoparticles, which predominantly exhibit electric dipole resonances, high-index silicon nanocubes provide both electric and magnetic dipole resonances within the visible spectrum, and their overlap generates superchiral fields within the gap of the silicon nanocube dimers. By adeptly employing the third Stokes parameter as a far-field probe, we effectively discern the presence of the local superchiral fields. Furthermore, we use the achiral silicon metasurfaces to detect enantiomers at concentrations as low as 5 $\mu g/ml$, showcasing very good sensitivity in solution while most detection on CD signal was done with a solid molecule layer. By comparison, it is easier to measure in solution environment. The observed CD signals in the presence of metasurfaces are about 12 times higher than those in the control samples. Our work not only provides deep insights into the intriguing chiral light-matter interactions but also lays a foundation for detecting enantiomers at low concentrations. By employing novel photonic nanostructure designs and innovative techniques such as optical trapping and specialized localization methods, we could further develop in-situ chiral sensing at even lower concentrations.

Acknowledgments

Y. L. acknowledges the support of the National Science Foundation (CBET-1931777 and 2323908). Z. D. would like to acknowledge the funding support from The National Research Foundation (NRF), Singapore via Grant No. NRF-CRP30-2023-0003, and the Agency for Science, Technology and Research (A*STAR) under its MTC IRG (Project No. M21K2c0116 and M22K2c0088).

References

[1] B. S. Sekhon, *Journal of Pesticide Science* **2009**, *34*, 1.
[2] L. A. Nguyen, H. He, C. Pham-Huy, *Int J Biomed Sci* **2006**, *2*, 85.
[3] A. J. Hutt, S. C. Tan, *Drugs* **1996**, *52*, 1.
[4] E. J. Ariëns, *Eur J Clin Pharmacol* **1984**, *26*, 663.
[5] L. D. Barron, *Molecular Light Scattering and Optical Activity*, Cambridge Univ. Press, Cambridge, **2009**.
[6] Y. Tang, A. E. Cohen, *Science* **2011**, *332*, 333.
[7] E. Mohammadi, K. L. Tsakmakidis, A. N. Askarpour, P. Dehkhoda, A. Tavakoli, H. Altug, *ACS Photonics* **2018**, *5*, 2669.
[8] G. Palermo, G. E. Lio, M. Esposito, L. Ricciardi, M. Manoccio, V. Tasco, A. Passaseo, A. De Luca, G. Strangi, *ACS Appl. Mater. Interfaces* **2020**, *12*, 30181.
[9] S. Jahani, Z. Jacob, *Nature Nanotech* **2016**, *11*, 23.
[10] A. I. Kuznetsov, A. E. Miroshnichenko, M. L. Brongersma, Y. S. Kivshar, B. Luk'yanchuk, *Science* **2016**, *354*, aag2472.
[11] E. Hendry, T. Carpy, J. Johnston, M. Popland, R. V. Mikhaylovskiy, A. J. Lapthorn, S. M. Kelly, L. D. Barron, N. Gadegaard, M. Kadodwala, *Nature Nanotech* **2010**, *5*, 783.
[12] N. A. Abdulrahman, Z. Fan, T. Tonooka, S. M. Kelly, N. Gadegaard, E. Hendry, A. O. Govorov, M. Kadodwala, *Nano Lett.* **2012**, *12*, 977.
[13] M. Schäferling, D. Dregely, M. Hentschel, H. Giessen, *Phys. Rev. X* **2012**, *2*, 031010.
[14] T. Iida, A. Ishikawa, T. Tanaka, A. Muranaka, M. Uchiyama, Y. Hayashi, K. Tsuruta, *Appl. Phys. Lett.* **2020**, *117*, 101103.
[15] X. Tian, Y. Fang, M. Sun, *Sci Rep* **2015**, *5*, 17534.
[16] S. Lee, S. Yoo, Q.-H. Park, *ACS Photonics* **2017**, *4*, 2047.
[17] M. L. Nesterov, X. Yin, M. Schäferling, H. Giessen, T. Weiss, *ACS Photonics* **2016**, *3*, 578.
[18] W. Zhang, T. Wu, R. Wang, X. Zhang, *J. Phys. Chem. C* **2017**, *121*, 666.
[19] S. Zu, Y. Bao, Z. Fang, *Nanoscale* **2016**, *8*, 3900.
[20] R. Adato, H. Altug, *Nat Commun* **2013**, *4*, 2154.
[21] M. H. Alizadeh, B. M. Reinhard, *ACS Photonics* **2015**, *2*, 361.
[22] M. Schäferling, X. Yin, H. Giessen, *Opt. Express* **2012**, *20*, 26326.
[23] P. Biagioni, M. Savoini, J.-S. Huang, L. Duò, M. Finazzi, B. Hecht, *Phys. Rev. B* **2009**, *80*, 153409.
[24] M. L. Solomon, J. Hu, M. Lawrence, A. García-Etxarri, J. A. Dionne, *ACS Photonics* **2019**, *6*, 43.
[25] A. García-Etxarri, J. A. Dionne, *Phys. Rev. B* **2013**, *87*, 235409.

[26] E. Mohammadi, A. Tavakoli, P. Dehkhoda, Y. Jahani, K. L. Tsakmakidis, A. Tittl, H. Altug, *ACS Photonics* **2019**, *6*, 1939.
[27] S. Yoo, Q.-H. Park, *Phys. Rev. Lett.* **2015**, *114*, 203003.
[28] R.-M. Ma, R. F. Oulton, *Nature Nanotech* **2019**, *14*, 12.
[29] A. E. Cetin, H. Altug, *ACS Nano* **2012**, *6*, 9989.
[30] M. L. Solomon, J. M. Abendroth, L. V. Poulikakos, J. Hu, J. A. Dionne, *J. Am. Chem. Soc.* **2020**, *142*, 18304.
[31] O. S. Wolfbeis, *Journal of Materials Chemistry* **2005**, *15*, 2657.
[32] H. Matsushita, N. Yamamoto, M. M. Meijler, P. Wirsching, R. A. Lerner, M. Matsushita, K. D. Janda, *Molecular BioSystems* **2005**, *1*, 303.
[33] Y. Zhao, H. Liu, B. Sun, *Sensors and Actuators B: Chemical* **2022**, *354*, 131253.
[34] K. Yao, Y. Liu, *Nanoscale* **2018**, *10*, 8779.
[35] K. Yao, Y. Zheng, *J. Phys. Chem. C* **2019**, *123*, 11814.
[36] R. Jin, X. Zhang, P. Huo, Z. Cai, Y. Lu, T. Xu, Y. Liu, *Phys. Rev. Lett.* **2024**, *133*, 086901.
[37] D. M. Lipkin, *Journal of Mathematical Physics* **1964**, *5*, 696.
[38] Y. Tang, A. E. Cohen, *Phys. Rev. Lett.* **2010**, *104*, 163901.
[39] L. V. Poulikakos, P. Thureja, A. Stollmann, E. De Leo, D. J. Norris, *Nano Lett.* **2018**, *18*, 4633.
[40] J. D. Jackson, *American Journal of Physics* **1999**, *67*, 841.
[41] L. V. Poulikakos, P. Gutsche, K. M. McPeak, S. Burger, J. Niegemann, C. Hafner, D. J. Norris, *ACS Photonics* **2016**, *3*, 1619.
[42] J. García-Guirado, M. Svedendahl, J. Puigdollers, R. Quidant, *Nano Lett.* **2020**, *20*, 585.